# Dependence of the energy of emission molecular orbitals in short open carbon nanotubes on the electric field

© *O.B. Tomilin*[1]*, E.V. Rodionova*[1,¶]*, E.A. Rodin*[1]*, N.A. Poklonski*[2]*, I.I. Anikeev*[2]*, S.V. Ratkevich*[2]

[1] Ogarev Mordovia State University,
Saransk, Russia
[2] Belarusian State University,
Minsk, Republic of Belarus

[¶] E-mail: Rodionova_j87@mail.ru

On the examples of short open carbon nanotubes of armchair type $(n, n)$, for $n = 3$, 4, and zigzag $(n, 0)$, for $n = 5$, 6, 7, the influence of the magnitude and direction of the external constant electric field vector on their field emission properties was studied. It is shown that the deviation of the field vector from the nanotube axis leads to an increase in the field strength to generate electron field emission. Emission orbitals in carbon nanotubes $(n, n)$ found as a result of a new type of conjugation of $p$-electrons in cylindrical conjugated systems are more sensitive to a change in the direction of the electric field vector compared to emission orbitals in nanotubes $(n, 0)$. When the electric field vector deviates from the nanotube axis, the emission orbitals of carbon nanotubes change the less, the larger the nanotube diameter.

**Keywords:** short open carbon nanotubes, field emission, conjugation of $p$-electrons, emission molecular orbital.

## 1. Introduction

Field-emission cathodes based on single-walled carbon nanotubes (CNTs) have a number of advantages over other pointed cathodes [1,2]: high emission current density, low turn-off voltage, high melting point, radiation resistance. The widespread use of carbon nanotubes in vacuum microelectronics is largely determined by the morphology of the cathode material, which is determined by the method of its synthesis and subsequent processing of the obtained arrays of CNTs. It has been experimentally shown [2] that spatially structured CNTs in the form of a „forest" exhibit better emission properties than randomly stacked CNTs. However, theoretical studies of the effect of CNT morphology in a cathode material on their emission properties are fragmentary [3,4] and do not contain results that can be considered recommendations for practical use. This position is largely determined by the lack of an accepted concept relating the electronic structure of carbon nanotubes and their emission properties. Thus, research in the field of predicting the emission properties of individual nanotubes and arrays of them remains relevant [5].

Most of the works devoted to both theoretical modeling of the field emission of electrons and interpretation of experimental data use the Fowler−Nordheim (FN) theory [6]. Usually, the classical theory of FN is adapted for CNTs by introducing various fitting coefficients [3]. The papers [7,8] present a new addition to the FN theory, which makes it possible to take into account the effect of real structural features of nanotubes, namely: the presence of caps on

the ends of CNTs, intrinsic defects, impurity atoms, or functional groups — on the emission properties of CNTs.

According to modern concepts of electronic conjugation in spherical and cylindrical molecules [9–13], a special type of $p$-electron conjugation is realized in single-walled carbon nanotubes — in-plane electronic conjugation. In contrast to the classical $\pi$-electronic conjugation, the in-plane electronic conjugation in spherical and cylindrical carbon macromolecules provides such an orientation of the $p$-orbitals with respect to carbon core, which causes an increased electron density inside the molecule. To minimize the total energy of molecules with in-plane electronic conjugation, „expulsion" of electron density from the inner cavity of the nanotube occurs, leading to the formation of new special molecular states — emission molecular orbitals (EMO) [7,8]. In other words, the formation of EMO due to the curvature of the surface of single-walled carbon nanotubes is a redistribution of the density of $p$-electrons from the inner region of CNTs outward to their outer surface [14]. A similar redistribution of the density of $p$-electrons (from the concave side to the convex one) also takes place when the graphene sheet is bent [15]. Thus, the lateral surface of CNTs also has crystallographic prerequisites for the formation of EMO.

A characteristic feature of the EMO of carbon nanotubes is the preferential localization of the electron density near the end surfaces of the cylindrical molecule. In [16] it is shown that the length of the region of preferential localization of electron density in CNTs is $4-5.5$ Å counted from the edge of the nanotube. The resulting emission

molecular orbitals are vacant [7], their occupancy will be determined only by the temperature and therefore have an insignificant value. This circumstance causes low field emission current densities at low electric field strength [17]. At the same time, such an EMO state can serve as a physical basis for interpreting the emission of electrons from CNT arrays under the action of intense visible light [18].

It was shown in [7] that a uniform constant electric field, whose field lines are parallel to the CNT axis, causes a change in the EMO energy, leading to the displacement of emission molecular orbitals to the valence band (i.e., to the region occupied by molecular orbitals). At a certain critical value of the electric field strength, the EMO is filled with valence band electrons, which is the physical basis for a sharp increase in the current density of cold field emission [17] due to the tunneling of EMO electrons through a potential barrier in accordance with the FN theory [3,6].

The presented mechanism of field emission from CNTs was successfully tested on the example of ultrashort CNTs in an electric field with a parallel orientation of the field vector and the axis of nanotubes [7]. Different methods of CNT synthesis generate materials with different nanotube morphology [2,19,20]. In addition, for different devices, the shape of the electrodes can vary widely, and, therefore, the electric field lines can be directed at different angles to the axis of the nanotubes. The purpose of this work is to study the influence of the direction and magnitude of the external constant electric field vector on the energies of emission molecular orbitals in carbon nanotubes $(3,3)$ and $(5,0)$.

## 2. Model and calculation method

In this work, ultrashort open single-layer (single-walled) carbon nanotubes of chirality $(n, 0)$ were chosen as objects of study, where $n = 5, 6, 7$ and $(n, n)$, where $n = 3, 4$. Closed CNTs were not studied in this work, since their emission properties are much inferior to those of open nanotubes [7]. The length of the model CNTs was 6 cyclic trans- and cis-carbon chains forming a cylindrical carbon core. The free valences of the terminal carbon atoms in the nanotubes were saturated with hydrogen atoms.

The spatial structure of the model CNTs was determined by optimization using the Hartree−Fock method in the 3-21G basis from the FireFly application package [21], and then the energy spectra of these CNTs were calculated.

The effect of a uniform constant electric field on the energy spectrum of the considered model CNTs was numerically simulated using the EFIELD option [21]. The strength $E$ of the constant electric field was varied within $0-21$ V/nm with a step of 1 V/nm. The constant electric field vector was directed at an angle $\Theta$ relative to the nanotube axis (Fig. 1). The angle $\Theta$ varied from $0°$ (the field vector is directed along the CNT axis) to $90°$ (the field
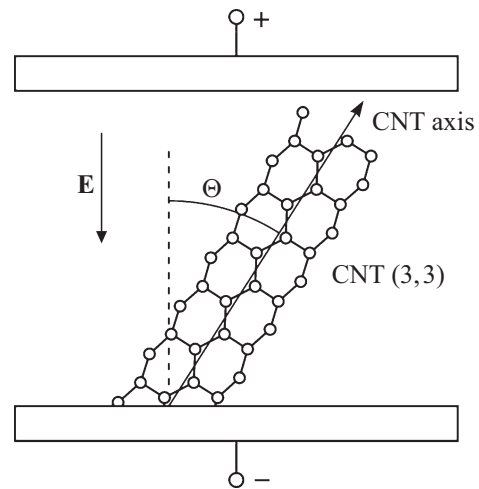


**Figure 1.** Direction of the vector of the external uniform constant electric field **E** to the carbon nanotube axis $(3, 3)$.

vector is directed perpendicular to the CNT axis) with a step of $15°$.

## 3. Discussion of results

In the energy spectrum of carbon nanotubes, there are several groups of emission orbitals that differ in the number of nodes $L$ of sign inversion of atomic wave functions in the basic EMO expansion (see Fig. 2). The first group (I) of emission orbitals is represented by two vacant energy-degenerate molecular orbitals (MOs) with $L = 2$. The second group (II) consists of four vacant energy-degenerate MOs with $L = 4$. The EMO energy increases with the growth of the number $L$. Therefore, the emission orbitals of the third group (III) with $L = 8$ lie deep in the valence band and do not significantly affect the emission properties of CNTs in the indicated range of electric field strength.

Figure 3 shows the energy dependences of the boundary (upper filled with electrons — HOMO and lower vacant — LUMO) and emission (EMO) molecular orbitals of model carbon nanotubes $(3,3)$ and $(5,0)$ on the constant electric field strength $E$ the strength vector of which is directed at an angle $\Theta$ to the axis of the CNTs.

In the case of $\Theta = 0°$, the applied electric field has the greatest effect on the energies of the emission orbitals $(\varepsilon_{EMO})$, while the energies of HOMO $(\varepsilon_{HOMO})$ and LUMO $(\varepsilon_{LUMO})$ orbitals change to a lesser extent. Let us consider the behavior of EMO in an electric field on the example of emission orbitals with $L = 2$. In an electric field, in accordance with the Stark effect [11–13], the energy-degenerate emission orbitals $EMO_1$ and $EMO_2$ are split. The energy of one of the $EMO_1$ emission orbitals decreases, and at a certain value of the field strength, the EMO energy reaches the LUMO energy, and then, at $E = E_{cr}^{I}$ — HOMO energy value. The energy of the second emission orbital $EMO_2$ increases significantly with increasing electric field
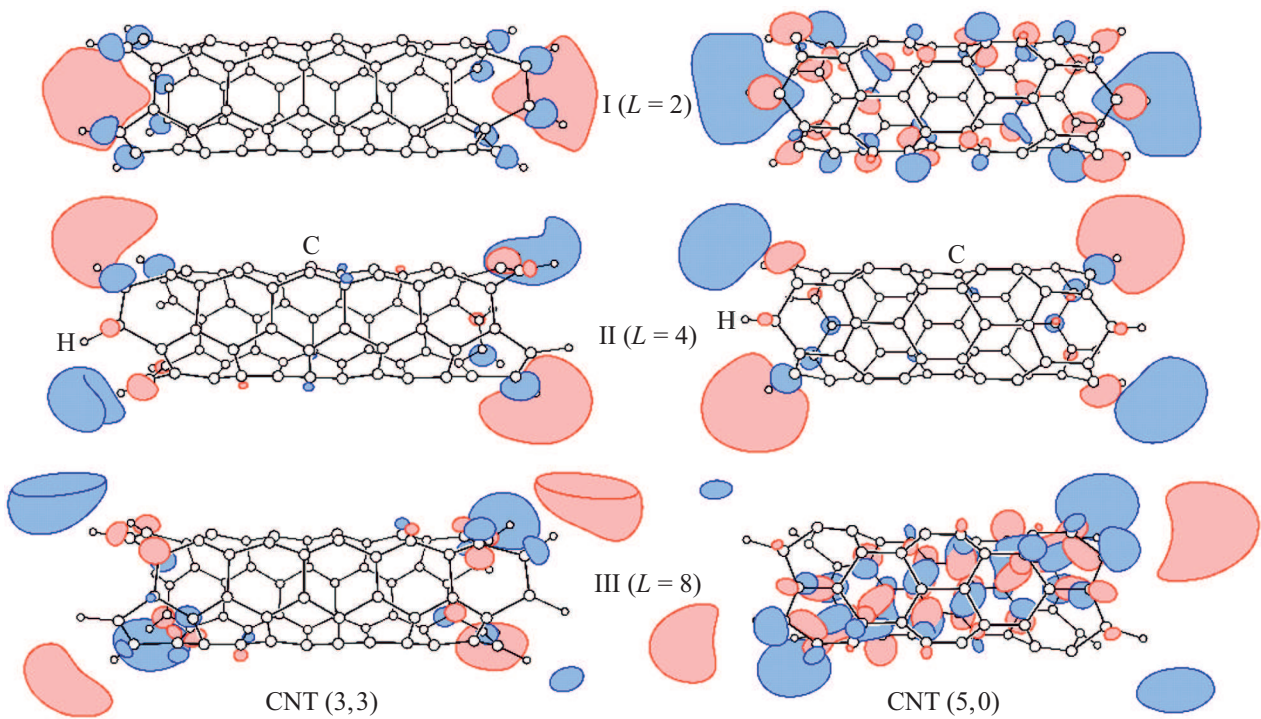
**Figure 2.** Structure of emission molecular orbitals in CNTs $(3,3)$ and $(5,0)$.
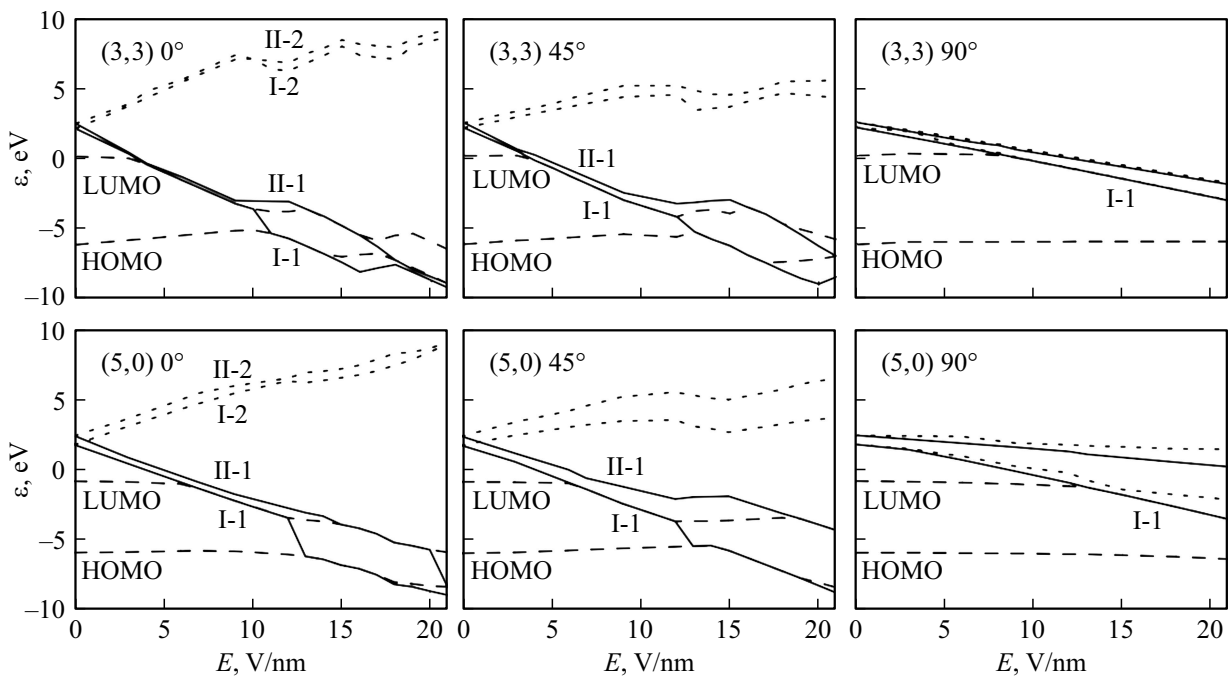


**Figure 3.** Energy dependences of the boundary (HOMO and LUMO) and emission (I-1(2) — $EMO_{I-1(2)}$, II-1(2) — $EMO_{II-1(2)}$) of CNT molecular orbitals $(3,3)$ and $(5,0)$ on the field strength $E$ of the external electric field at $\Theta = 0°$, $45°$ and $90°$.

strength and is of no interest in describing the emission properties of CNTs. The behavior of the emission orbitals with $L = 4$ is similar to the behavior of the EMO with $L = 2$. Thus, at an electric field strength of $E_{cr}^{II}$, the value of the EMO energy with $L = 4$ reaches the value of the

HOMO energy. This circumstance qualitatively explains the increase in the emission current with increasing applied field strength [3–5].

When the electric field vector deviates from the nanotube axis, the regularities in the behavior of the energy of frontier
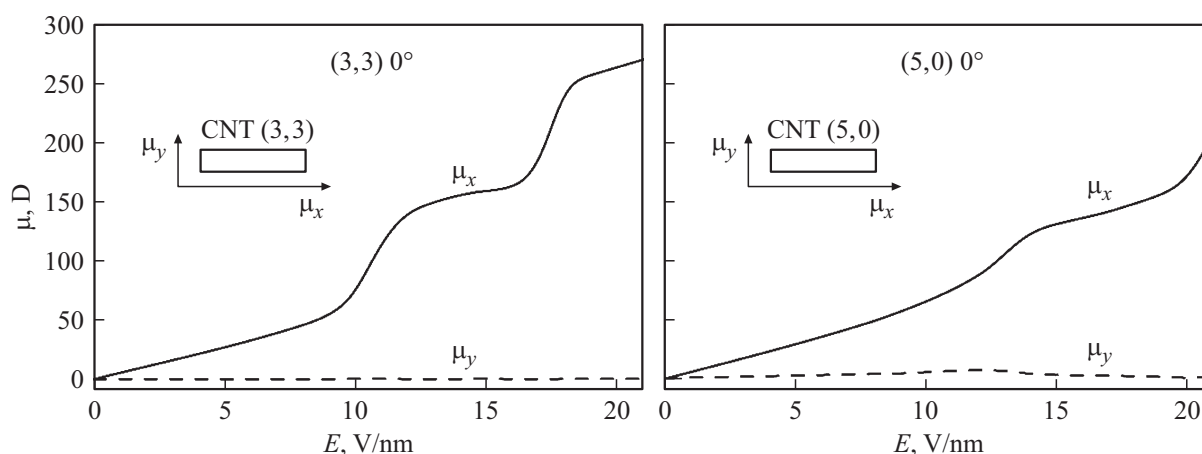
**Figure 4.** Dependence of the projections $\mu_x$ and $\mu_y$ of the induced CNT dipole moment $(3,3)$ and $(5,0)$ on the strength $E$ of the external electric field (at $\Theta = 0°$). The magnitude of the dipole moment is given in debyes; $1\,\text{D} = 3.34 \cdot 10^{-30}\,\text{C}\cdot\text{m}$.

orbitals and $EMO_1$ remain unchanged with increasing field strength (Fig. 3), and the EMO splitting will decrease. The degeneracy of the EMO is completely preserved at $\Theta = 90°$ due to the equivalence of the EMO for the indicated direction of the electric field and the decrease in the dipole moment of CNTs.

Let us trace the influence of the quantity $\Theta$ on the critical values of the external electric field strength ($E_{cr}^I$ and $E_{cr}^{II}$). It can be seen from the table that the critical values of the field strength providing electron field emission at comparable radii for armchair-type CNTs are smaller than for zigzag-type CNTs, which corresponds to the data [22].

For all considered model CNTs, as the angle $\Theta$ increases, the electron field emission region shifts towards stronger fields. At $\Theta = 90°$ in the range of electric fields up to 20 V/nm, no EMO transition to the valence band is observed. Unlike CNTs of chirality $(n, 0)$, the emission properties of model nanotubes of chirality $(n, n)$ turned out to be more sensitive to the direction of the electric field

vector relative to the CNT axis. Thus, the values of the critical field strength, which ensure the filling of the EMO ($L = 2$) with electrons, for CNT $(n, 0)$ begin to increase at $\Theta = 60°$, while $E_{cr}^I$ CNT $(n, n)$ tend to increase even at $\Theta = 45°$. The results obtained are in agreement with the data on the dependence of the electric field amplification factor at the end of the CNT on the direction of the field vector determined in the work [23]. An increase in the diameter of model nanotubes affects the $E_{cr}$ values to a lesser extent. Thus, for $\Theta > 60°$, „equalization" of the emission properties of nanotubes of different chirality and diameters is observed. In addition, an increase in the diameter of zigzag CNTs reduces the number of emission orbitals in the valence band, which leads to a decrease in the emission current.

The redistribution of the electron density between molecular orbitals, taking into account the EMO formed by a new type of conjugation of $p$-electrons in cylindrical molecules, can be considered by studying the dipole moment $\boldsymbol{\mu}$ of CNTs by the action of an electric field. The vector of the

Values of the critical electric field strength that ensure the transition of emission orbitals to LUMO and HOMO, for model CNTs $(n, 0)$ and $(n, n)$ depending on the angle $\Theta$

| Angle $\Theta$, deg | CNT chirality index | | | | | | | | | |
|---|---|---|---|---|---|---|---|---|---|---|
| | $(5,0)$ | | $(6,0)$ | | $(7,0)$ | | $(3,3)$ | | $(4,4)$ | |
| Radius, nm | 0.196 | | 0.235 | | 0.274 | | 0.203 | | 0.271 | |
| | $E_{cr}^I$, V/nm | $E_{cr}^{II}$, V/nm | $E_{cr}^I$, V/nm | $E_{cr}^{II}$, V/nm | $E_{cr}^I$, V/nm | $E_{cr}^{II}$, V/nm | $E_{cr}^I$, V/nm | $E_{cr}^{II}$, V/nm | $E_{cr}^I$, V/nm | $E_{cr}^{II}$, V/nm |
| 0 | 13 | 21 | 18 | − | 20 | − | 11 | 18 | 11 | 18 |
| 15 | 13 | 21 | 18 | − | 20 | − | 11 | 18 | 11 | 18 |
| 30 | 13 | − | 18 | − | 20 | − | 11 | 19 | 11 | 19 |
| 45 | 13 | − | 18 | − | 20 | − | 13 | 21 | 12 | 21 |
| 60 | 15 | − | 20 | − | 21 | − | 15 | − | 14 | − |
| 75 | 19 | − | 21 | − | 21 | − | 18 | − | 18 | − |
| 90 | − | − | − | − | − | − | − | − | − | − |

**Figure 5.** Dependencies of the derivatives of the projections of the CNT dipole moment $(3, 3)$ and $(5, 0)$ on the strength $E$ of the external electric field.

dipole moment induced in the electric field can be expanded into projections along the axes $x$ (along the nanotube axis) and $y$ (across the nanotube axis). The projection $\mu_x$ of the dipole moment $\boldsymbol{\mu}$ onto the $x$ axis characterizes the longitudinal polarizability of CNTs, and the projection $\mu_y$ onto the $y$ axis — transverse polarizability (Fig. 4).

A significant redistribution of the electron density of CNTs in an electric field is evidenced by a nonmonotonic increase in the dipole moment with an increase in the electric field strength. At $\Theta = 0°$, the main contribution to the total CNT dipole moment comes from its „longitudinal" projection $\mu_x$. An increase in the strength of the external electric field leads to an increase in the dipole moment.

Figure 5 shows the dependence of the derivative of the dipole moment with respect to the field strength $d\boldsymbol{\mu}/d\mathbf{E} = \boldsymbol{\mu}'$ on the field strength $\mathbf{E}$. An analysis of these dependences shows that the maxima $\boldsymbol{\mu}'$ correspond to an additional redistribution of charges in CNTs that occurs in excess of the usual polarizability. Thus, for a CNT $(3, 3)$ oriented along the direction of the external electric field (at $\Theta = 0°$), the maximum at $E = 11$ V/nm corresponds to the transition of the emission molecular orbital $(L = 2)$ at the edge of the valence band, the filling of this EMO with electrons and, consequently, the accumulation of electron density in the end region of the nanotube. The second maximum is associated with the transition of the next EMO $(L = 4)$ to the edge of the valence band at $E = 18$ V/nm. Similar transformations of the EMO energy $(L = 2$ and $L = 4)$ in the CNT energy spectrum $(5, 0)$ also lead to the appearance of maxima at $E = E_{\mathrm{cr}}^{\mathrm{I}}$ and $E = E_{\mathrm{cr}}^{\mathrm{II}}$.

As the angle $\Theta$ increases, the contribution of „the transverse" projection of the dipole moment $\mu_y$ to the total dipole moment increases. At the same time, the CNT dipole moment at a given field strength decreases with increasing angle $\Theta$, practically disappearing at $\Theta = 90°$.

## 4. Conclusion

The emission characteristics of cathodes based on carbon nanotubes significantly depend on the morphology of the materials used. Thus, when forming large-area cathodes by printing technologies, the resulting coatings are characterized by an extremely low degree of order of CNTs [4,20]. For the manufacture of such cathodes, nanotubes of any chirality and diameter can be used, since the emission properties of CNTs in arrays with a low degree of order „are averaged".

At the same time, it is preferable to form arrays with a high degree of ordering of CNTs obtained using the „forest" technology [2] from armchair-type nanotubes, since for them the critical strength of the field for the appearance of cold electron emission $(E_{\mathrm{cr}}^{\mathrm{I}})$ is smaller than for zigzag-type CNT arrays at comparable nanotube radii. In addition, armchair-type nanotube cathodes have stable emission characteristics, regardless of the radius of the CNTs used.

**Conflict of interest**

The authors declare that they have no conflict of interest.

## Funding

## References

[1] I.D. Evsikov, S.V. Mit'ko, P.Yu. Glagolev, N.A. Dyuzhev, G.D. Demin. Technical Physics **65**, *11*, 1846 (2020). https://doi.org/10.1134/S1063784220110067

[2] E.G. Rakov. Russ. Chem. Rev. **82**, *6*, 538 (2013). https://doi.org/10.1070/RC2013v082n06ABEH004340

[3] A.V. Eletskii. Physics-Uspekhi **53**, *9*, 863 (2010). https://iopscience.iop.org/article/10.3367/UFNe.0180.201009a.0897

[4] F. Giubileo, A. Di Bartolomeo, L. Iemmo, G. Luongo, F. Urban. Appl. Sci. **8**, *4*, 526 (2018). https://doi.org/10.3390/app8040526

[5] E.D. Eidelman, A.V. Arkhipov. Physics-Uspekhi **63**, *7*, 648 (2020). https://iopscience.iop.org/article/10.3367/UFNe.2019.06.038576

[6] S. Parveen, A. Kumar, S. Husain, M. Husain. Physica B **505**, 1 (2017). https://doi.org/10.1016/j.physb.2016.10.031

[7] O.B. Tomilin, E.V. Rodionova, E.A. Rodin. Russ. J. Phys. Chem. A **94**, *8*, 1657 (2020). https://doi.org/10.1134/S0036024420080269

[8] O.B. Tomilin, E.V. Rodionova, E.A. Rodin. Russ. J. Phys. Chem. A **95**, *9*, 1883 (2021). https://doi.org/10.1134/S0036024421090296

[9] P. von Ragué Schleyer, H. Jiao, M.N. Glukhovtsev, J. Chandrasekhar, E. Kraka. J. Am. Chem. Soc. **116**, *22*, 10129 (1994). https://doi.org/10.1021/ja00101a035

[10] A.A. Fokin, H. Jiao, P. von Ragué Schleyer. J. Am. Chem. Soc. **120**, *36*, 9364 (1998). https://doi.org/10.1021/ja9810437

[11] A.V. Tuchin, L.A. Bityutskaya, E.N. Bormontov. Nano- i mikrosistemnaya tekhnika, **4**, 19 (2013) (in Russian). http://www.microsystems.ru/files/publ/article201304p19-21.pdf

[12] A.V. Tuchin, L.A. Bityutskaya, E.N. Bormontov. Physics of the Solid State **56**, *8*, 1685 (2014). https://doi.org/10.1134/S1063783414080277

[13] R.I. Gearba, T. Mills, J. Morris, R. Pindak, C.T. Black, X. Zhu. Adv. Funct. Mater. **21**, *14*, 2666 (2011). https://doi.org/10.1134/S1063783414080277

[14] T. Dumitrică, Ch.M. Landis, B.I. Yakobson. Chem. Phys. Lett. **360**, *1−2*, 182 (2002). https://doi.org/10.1016/S0009-2614(02)00820-5

[15] N.A. Poklonski, S.V. Ratkevich, S.A. Vyrko, A.T. Vlassov. Int. J. Nanosci. **18**, *03n04*, 1940008 (2019). https://doi.org/10.1142/S0219581X19400088

[16] O.B. Tomilin, N.A. Poklonski, E.V. Rodionova, E.A. Rodin, I.I. Anikeev, V.A. Kushnerov, A.S. Chitalov. Materialy i struktury sovremennoy elektroniki. Materialy IX Mezhdunar. nauch. konf. (14−16 Oct. 2020) BSU, Minsk (2020). P. 406 (in Russian). https://elib.bsu.by/handle/123456789/257358

[17] S. Han, J. Ihm. Phys. Rev. B **66**, *24*, 241402(R) (2002). https://doi.org/10.1103/PhysRevB.66.241402

[18] P. Yaghoobi, M.V. Moghaddam, A. Nojeh. In: 23rd Int. Vacuum Nanoelectronic Conf. Palo Alto, CA (2010). P. 115 https://doi.org/10.1109/IVNC.2010.5563199

[19] A. Navitski, G. Müller, V. Sakharuk, A.L. Prudnikava, B.G. Shulitski, V.A. Labunov. J. Vac. Sci. Technol. B **28**, *2*, C2B14 (2010). http://dx.doi.org/10.1116/1.3300062

[20] J.-W. Song, Y.-S. Kim, Y.-H. Yoon, E.-S. Lee, C.-S. Han, Y. Cho, D. Kim, J. Kim, N. Lee, Y.-G. Ko, H.-T. Jung, S.-H. Kim. Physica E **41**, *8*, 1513 (2009). https://doi.org/10.1016/j.physe.2009.04.031

[21] M.W. Schmidt, K.K. Baldridge, J.A. Boatz, S.T. Elbert, M.S. Gordon, J.H. Jensen, S. Koseki, N. Matsunaga, K.A. Nguyen, S. Su, T.L. Windus, M. Dupuis, J.A. Montgomery. J. Comp. Chem. **14**, *11*, 1347 (1993). https://doi.org/10.1002/jcc.540141112

[22] A.G. Rinzler, J.H. Hafner, P. Nikolaev, P. Nordlander, D.T. Colbert, R.E. Smalley, L. Lou, S.G. Kim, D. Tománek. Science **269**, *5230*, 1550 (1995). https://doi.org/10.1126/science.269.5230.1550

[23] M.D. Bel'skii, G.S. Bocharov, A.V. Eletskii, T.J. Sommerer. Technical Physics **55**, *2*, 289 (2010). https://doi.org/10.1134/S1063784210020210